Four-phonon scattering reduces intrinsic thermal conductivity of graphene and the contributions from flexural phonons

Tianli Feng and Xiulin Ruan

Phys. Rev. B **97**, 045202 — Published 5 January 2018

DOI: 10.1103/PhysRevB.97.045202

Four-phonon scattering reduces thermal conductivity in graphene and the contributions from flexural phonons

Tianli Feng[1] and Xiulin Ruan[1,*]

[1] *School of Mechanical Engineering and the Birck Nanotechnology Center, Purdue University, West Lafayette, Indiana 47907-2088, USA*

(Dated: December 5, 2017)

We have developed a formalism of the exact solution to linearized phonon Boltzmann transport equation (BTE) for thermal conductivity calculation including three- and four-phonon scattering. We find strikingly high four-phonon scattering rates in single-layer graphene (SLG) based on the optimized Tersoff potential. The reflection symmetry in graphene, which forbids the three-ZA (out-of-plane acoustic) scattering, allows the four-ZA processes ZA+ZA⇌ZA+ZA and ZA⇌ZA+ZA+ZA. As a result, the large phonon population of the low-energy ZA branch originated from the quadratic phonon dispersion leads to high four-phonon scattering rates, even much higher than the three-phonon scattering rates at room temperature. These four-phonon processes are dominated by the Normal processes, which lead to a failure of the single mode relaxation time approximation. Therefore, we have solved the exact phonon BTE using an iterative scheme and then calculated the length- and temperature-dependent thermal conductivity. We find that the predicted thermal conductivity of SLG is lower than the previously predicted value from the three-phonon scattering only. The relative contribution of the ZA branch is reduced from 70% to 30% when four-phonon scattering is included, consistent with molecular dynamics simulations. Furthermore, we have demonstrated that the four-phonon scattering in multi-layer graphene and graphite is not strong due to the ZA splitting by interlayer van der Waals interaction. We also demonstrate that the five-phonon process in SLG is not strong due to the reflection symmetry.

I. INTRODUCTION

Graphene has attracted intense interest for both fundamental research and practical applications [1–4] due to its unique structure and extraordinary properties. The two-dimensional honeycomb structure, zero bandgap and strong sp^2 bond endow graphene with unique electronic[5,6], thermal [7–9], optical [10] and mechanical [11] behaviors. For instance, the high mobility and long phonon mean free path result in small heat generation and a high thermal conductivity [8,9,12–14], which is potentially helpful for heat dissipation in nano devices with shrinking package sizes [15].

Extensive theoretical studies have been carried out to explain the high thermal conductivity and to gain insight into the spectral phonon transport [2,3,16] in single-layer graphene (SLG). Lindsay and co-workers optimized the classical C-C interatomic potentials and obtained the phonon dispersions and anharmonic properties which agree excellently with first principle calculations based on the density functional theory (DFT) [17]. Molecular dynamics (MD) simulations based on the optimized potentials yield a thermal conductivity of 1100-2900 W/mK for graphene at room temperature [18–20], which agrees better with the experimental values. Nevertheless, the classical MD simulation results need to be used with caution due to the ignorance of quantum effects in specific heat and the phonon distribution function since the room temperature is far below the Debye temperature of graphene, which is about 1000-2300 K [21]. More precisely, Lindsay and co-workers [22,23] solved the linearized BTE based on the third-order interatomic force constants (IFCs) and obtained a size dependent thermal conductivity of graphene of 1500-3500 W/mK for 1-10 μm. They found that although the Normal (N) scattering does not contribute directly to thermal resistance it can significantly affect the Umklapp (U) scattering and thus plays an important role in determining thermal conductivity. Besides, they identified the reflection symmetry in single-layer graphene and found that it could restrict the phase space for parts of the scattering between the out-of-plane modes and in-plane modes. As a result, ZA phonons have significantly long relaxation times and thus dominate the thermal transport, contributing to over 70% to the total thermal conductivity. In contrast, MD simulations only predicted 30% contributions from ZA [3,16,18,24,25].

Although BTE calculations avoid the limitation of the classical nature in MD simulations, they are still under debate since they only include three-phonon scattering in the calculation of phonon relaxation times. The ignorance of four-phonon scattering has been found to produce significant inaccuracy in anharmonic bulk materials [26,27]. It is interesting to find out the role of four-phonon scattering in the thermal transport in the two-dimensional material, graphene. The four-phonon scattering calculation formalism based on the single mode relaxation time approximation (SMRTA) has already been presented and applied to bulk materials in our previous work [26,27]. However, as indicated by Lindsay et al. [22,23], the SMRTA improperly takes N processes as a direct thermal resistant source and thus leads to an overestimation of scattering rates especially in the materials like graphene in which the N processes dominate. Thus, an iterative scheme has been developed to exactly solve the linearized phonon BTE to replace the SMRTA [16,28]. To address the importance of four-phonon scattering, it is necessary to include four-phonon scattering into the iterative scheme. However, the calculation of the SMRTA four-phonon scattering is already a large challenge [26,27], involving it into the iterative scheme could increase the challenge to an inaccessible level.

The manuscript is organized as follows. In Sec. II, we present the iterative method to exactly solve the linearized phonon BTE that includes four-phonon scattering. In Sec. III, we describe the setup of our calculations and demonstrate the technical details in the methods of enhancing the efficiency of

the calculations without losing any accuracy. In Sec. IV, we give the results and discussions including the role of the reflection symmetry in four-phonon scattering (IV A), the ultra-high four-phonon scattering rates in SLG (IV B), the dominant N processes in three- and four-phonon scattering (IV C), the thermal conductivity reduction after introducing the four-phonon scattering given by the iterative scheme (IV D), the relative thermal conductivity contribution of each branch (IV E), and further discussions on the four-phonon scattering in multi-layer graphene and graphite as well as the five-phonon process in SLG (IV F). The conclusions are given in Sec. V. In Appendix A, we show the details of the derivation of the solution to linearized phonon BTE. In Appendix B, we summarize the important Hamiltonians that determine the phonon scattering probabilities from the literature.

II. EXACT SOLUTION TO LINEARIZED PHONON BOLTZMANN TRANSPORT EQUATION

In the perturbation theory, the steady-state phonon BTE describes the balance of the phonon population between the diffusive drift and the scattering as [29–31]:

$$\mathbf{v}_\lambda \cdot \nabla n_\lambda = \frac{\partial n_\lambda}{\partial t}|_s, \tag{1}$$

where λ labels the phonon mode ($\mathbf{k}$, ν) with $\mathbf{k}$ representing the wave vector and ν representing the dispersion branch, $\mathbf{v}_\lambda$ is the group velocity, and n_λ is the phonon occupation number. In Ref. [26], we have obtained the phonon relaxation time solution to Eq. (1) within the framework of the SMRTA by including the three-phonon and four-phonon scattering rates in the scattering term on the right hand side of Eq. (1). However, when N processes dominate the phonon transport, which reaches a collective regime with non-equilibrium distribution [32], the SMRTA is not appropriate anymore. Such a phenomenon results from the fact that the N processes contribute indirectly to the thermal resistance by influencing the U processes. And thus, a direct summation of the N and U scattering rates in the SMRTA is an inaccurate description of the thermal resistance. At this stage, an exact solution to the linearized phonon BTE [22,28,33] beyond the SMRTA is required.

For generality, we include the three-phonon, four-phonon, isotope, and boundary scattering processes in the scattering term on the right hand side of Eq. (1). With the detailed derivation given in the Appendices A and B, the final solution of the spectral phonon relaxation time is

$$\tau_\lambda = \tau_\lambda^0(1 + \Xi_{3,\lambda} + \Xi_{4,\lambda} + \Xi_{iso,\lambda}). \tag{2}$$

Here τ_λ^0 is the SMRTA based phonon relaxation time [26] with

$$\frac{1}{\tau_\lambda^0} = \frac{1}{\tau_{3,\lambda}^0} + \frac{1}{\tau_{4,\lambda}^0} + \frac{1}{\tau_{iso,\lambda}^0} + \frac{1}{\tau_{b,\lambda}^0}, \tag{3}$$

which consists of the SMRTA based individual three-phonon, four-phonon, isotope and boundary scattering rates

$$\frac{1}{\tau_{3,\lambda}^0} = \sum_{\lambda'\lambda''} \left\{ \frac{1}{2}(1 + n_{\lambda'}^0 + n_{\lambda''}^0)\mathcal{L}_- + (n_{\lambda'}^0 - n_{\lambda''}^0)\mathcal{L}_+ \right\}, \tag{4}$$

$$\frac{1}{\tau_{4,\lambda}^0} = \sum_{\lambda'\lambda''\lambda'''} \left\{ \frac{1}{6}\frac{n_{\lambda'}^0 n_{\lambda''}^0 n_{\lambda'''}^0}{n_\lambda^0}\mathcal{L}_{--} + \frac{1}{2}\frac{(1+n_{\lambda'}^0)n_{\lambda''}^0 n_{\lambda'''}^0}{n_\lambda^0}\mathcal{L}_{+-} + \frac{1}{2}\frac{(1+n_{\lambda'}^0)(1+n_{\lambda''}^0)n_{\lambda'''}^0}{n_\lambda^0}\mathcal{L}_{++} \right\}, \tag{5}$$

$$\frac{1}{\tau_{iso,\lambda}^0} = \sum_{\lambda'} \mathcal{L}_{iso}, \tag{6}$$

$$\frac{1}{\tau_{b,\lambda}^0} = \frac{2|v_{\lambda,x}|}{L} + \frac{2|v_{\lambda,y}|}{W}\frac{1-p}{1+p}, \tag{7}$$

where $n_\lambda^0 = [\exp(\hbar\omega_\lambda/k_BT)-1]^{-1}$ is the phonon Bose-Einstein distribution function. In Eq. (4), the two terms on the right hand side represent the processes $\lambda \rightarrow \lambda'+\lambda''$ and $\lambda+\lambda' \rightarrow \lambda''$, respectively. In Eq. (5), the three terms on the right hand side represent the processes $\lambda \rightarrow \lambda'+\lambda''+\lambda'''$, $\lambda+\lambda' \rightarrow \lambda''+\lambda'''$ and $\lambda+\lambda'+\lambda'' \rightarrow \lambda'''$, respectively. In Eq. (6), the right hand side indicates the elastic scattering process $\lambda \rightarrow \lambda'$. In Eq. (7), L and W represent the length and width of the material in the x and the y directions, respectively, assuming that the heat transport is along x direction. $0 \le p \le 1$ is the specularity parameter with $p = 0$ indicating the extremely rough boundary and $p = 1$ indicating the mirror-like boundary. $\Xi_{3,\lambda}$, $\Xi_{4,\lambda}$, and $\Xi_{iso,\lambda}$ are defined as

$$\Xi_{3,\lambda} = \sum_{\lambda'\lambda''} \left\{ \frac{1}{2}(\tau_{\lambda'}\xi_{\lambda\lambda'} + \tau_{\lambda''}\xi_{\lambda\lambda''})(1 + n_{\lambda'}^0 + n_{\lambda''}^0)\mathcal{L}_- + (\tau_{\lambda''}\xi_{\lambda\lambda''} - \tau_{\lambda'}\xi_{\lambda\lambda'})(n_{\lambda'}^0 - n_{\lambda''}^0)\mathcal{L}_+ \right\}, \tag{8}$$

$$\Xi_{4,\lambda} = \sum_{\lambda'\lambda''\lambda'''} \left\{ \frac{1}{6}(\tau_{\lambda'}\xi_{\lambda\lambda'} + \tau_{\lambda''}\xi_{\lambda\lambda''} + \tau_{\lambda'''}\xi_{\lambda\lambda'''})\frac{n_{\lambda'}^0 n_{\lambda''}^0 n_{\lambda'''}^0}{n_\lambda^0}\mathcal{L}_{--} + \frac{1}{2}(\tau_{\lambda''}\xi_{\lambda\lambda''} + \tau_{\lambda'''}\xi_{\lambda\lambda'''} - \tau_{\lambda'}\xi_{\lambda\lambda'})\frac{(1+n_{\lambda'}^0)n_{\lambda''}^0 n_{\lambda'''}^0}{n_\lambda^0}\mathcal{L}_{+-} + \frac{1}{2}(\tau_{\lambda'''}\xi_{\lambda\lambda'''} - \tau_{\lambda'}\xi_{\lambda\lambda'} - \tau_{\lambda''}\xi_{\lambda\lambda''})\frac{(1+n_{\lambda'}^0)(1+n_{\lambda''}^0)n_{\lambda'''}^0}{n_\lambda^0}\mathcal{L}_{++} \right\}, \tag{9}$$

$$\Xi_{iso,\lambda} = \sum_{\lambda'} \tau_{\lambda'}\xi_{\lambda\lambda'}\mathcal{L}_{iso}, \tag{10}$$

and $\xi_{\lambda\lambda'}$, $\xi_{\lambda\lambda''}$ and $\xi_{\lambda\lambda'''}$ are defined as

$$\xi_{\lambda\lambda'} \equiv \frac{\omega_{\lambda'}}{\omega_\lambda}\frac{\mathbf{v}_{\lambda'}\cdot\nabla T}{\mathbf{v}_\lambda\cdot\nabla T} = \frac{\omega_{\lambda'}v_{\lambda'x}}{\omega_\lambda v_{\lambda x}}, \tag{11}$$

$$\xi_{\lambda\lambda'} \equiv \frac{\omega_{\lambda'}}{\omega_\lambda}\frac{\mathbf{v}_{\lambda'}\cdot\nabla T}{\mathbf{v}_\lambda\cdot\nabla T} = \frac{\omega_{\lambda'}v_{\lambda' x}}{\omega_\lambda v_{\lambda x}}, \tag{12}$$

$$\xi_{\lambda\lambda''} \equiv \frac{\omega_{\lambda''}}{\omega_\lambda}\frac{\mathbf{v}_{\lambda''}\cdot\nabla T}{\mathbf{v}_\lambda\cdot\nabla T} = \frac{\omega_{\lambda''}v_{\lambda'' x}}{\omega_\lambda v_{\lambda x}}, \tag{13}$$

where $v_{\lambda x}$ is the phonon group velocity component in the heat transport x direction. Since both the left and the right hand sides contains the unknown τ_λ, Eq. (2) is solved iteratively and thus is also called the iterative scheme. The scattering probability matrices

$$\mathcal{L}_\pm = \frac{\pi\hbar}{4N}\left|V_\pm^{(3)}\right|^2\Delta_\pm\frac{\delta(\omega_\lambda\pm\omega_{\lambda'}-\omega_{\lambda''})}{\omega_\lambda\omega_{\lambda'}\omega_{\lambda''}}, \tag{14}$$

$$\mathcal{L}_{\pm\pm} = \frac{\pi\hbar}{4N}\frac{\hbar}{2N}\left|V_{\pm\pm}^{(4)}\right|^2\Delta_{\pm\pm}\frac{\delta(\omega_\lambda\pm\omega_{\lambda'}\pm\omega_{\lambda''}-\omega_{\lambda'''})}{\omega_\lambda\omega_{\lambda'}\omega_{\lambda''}\omega_{\lambda'''}}, \tag{15}$$

$$\mathcal{L}_{iso} = \frac{\pi}{2N}\omega_\lambda\omega_{\lambda'}\sum_b^n g_b|\mathbf{e}_b^\lambda\cdot\mathbf{e}_b^{\lambda'*}|^2\delta(\omega_\lambda-\omega_{\lambda'}), \tag{16}$$

are given by the Fermi's Golden Rule based on the corresponding Hamiltonians shown in Appendix B. N is the total number of $\mathbf{k}$-points or primitive cells. The Kronecker deltas $\Delta_\pm = \Delta_{\mathbf{k}\pm\mathbf{k}'-\mathbf{k}'',\mathbf{G}}$ and $\Delta_{\pm\pm} = \Delta_{\mathbf{k}\pm\mathbf{k}'\pm\mathbf{k}''-\mathbf{k}''',\mathbf{G}}$ describe the momentum selection rule (MSR) and have the property that $\Delta_{m,n} = 1$ (if $m = n$), or 0 (if $m \neq n$), where $\mathbf{G}$ is a reciprocal lattice vector with $\mathbf{G} = 0$ implying the Normal (N) process and $\mathbf{G} \neq 0$ the Umklapp (U) process. The delta functions in Eq. (14), (15) and (16) describe the energy selection rules (ESRs) $\omega_\lambda \pm \omega_{\lambda'} - \omega_{\lambda''} = 0$, $\omega_\lambda \pm \omega_{\lambda'} \pm \omega_{\lambda''} - \omega_{\lambda'''} = 0$, and $\omega_\lambda - \omega_{\lambda'} = 0$, respectively. In Eq. (16), $g_b = \sum_i f_{ib}(1 - m_{ib}/\bar{m}_b)^2$ measures the mass disorder, where i indicates the isotope types, f_{ib} is the fraction of the isotope i in the lattice sites of the basis atom b, m_{ib} is the mass of the isotope i, $\bar{m}_b$ is the average atom mass of the basis b sites. The transition probability matrices $V_\pm^{(3)}$ and $V_{\pm\pm}^{(4)}$ are

$$V_\pm^{(3)} = \sum_{b,l'b',l''b''}\sum_{\alpha\alpha'\alpha''}\Phi_{0b,l'b',l''b''}^{\alpha\alpha'\alpha''}\frac{e_{\alpha b}^{\lambda}e_{\alpha' b'}^{\pm\lambda'}e_{\alpha'' b''}^{-\lambda''}}{\sqrt{\bar{m}_b\bar{m}_{b'}\bar{m}_{b''}}}e^{\pm i\mathbf{k}'\mathbf{r}_{l'}}e^{-i\mathbf{k}''\mathbf{r}_{l''}}, \tag{17}$$

$$V_{\pm\pm}^{(4)} = \sum_{b,l'b',l''b'',l'''b'''}\sum_{\alpha\alpha'\alpha''\alpha'''}\Phi_{0b,l'b',l''b'',l'''b'''}^{\alpha\alpha'\alpha''\alpha'''}\frac{e_{\alpha b}^{\lambda}e_{\alpha' b'}^{\pm\lambda'}e_{\alpha'' b''}^{\pm\lambda''}e_{\alpha''' b'''}^{-\lambda'''}}{\sqrt{\bar{m}_b\bar{m}_{b'}\bar{m}_{b''}\bar{m}_{b'''}}}e^{\pm i\mathbf{k}'\cdot\mathbf{r}_{l'}}e^{\pm i\mathbf{k}''\cdot\mathbf{r}_{l''}}e^{-i\mathbf{k}'''\cdot\mathbf{r}_{l'''}}, \tag{18}$$

where b, l, and α label the indexes of the basis atoms, the unit cells, and the directions, respectively. $\Phi_{0b,l'b',l''b''}^{\alpha\alpha'\alpha''}$ and $\Phi_{0b,l'b',l''b'',l'''b'''}^{\alpha\alpha'\alpha''\alpha'''}$ are the third-order and the fourth-order interatomic force constants (IFCs). $e_{\alpha b}^{\lambda}$ is the phonon eigenvector component. $\mathbf{r}_l$ is the position vector of the lth unit cell. The phonon frequencies ω_λ and eigenvectors $\mathbf{e}$ are determined by diagonalizing the dynamical matrix

$$D_{bb'}^{\alpha\alpha'}(\mathbf{k}) = \frac{1}{\sqrt{m_b m_{b'}}}\sum_{l'}\Phi_{0b,l'b'}^{\alpha\alpha'}e^{i\mathbf{k}\cdot\mathbf{r}_{l'}}, \tag{19}$$

where $\Phi_{0b,l'b'}^{\alpha\alpha'}$ is the 2nd order IFC.

The thermal conductivity is given by

$$\kappa_x = \frac{1}{V}\sum_\lambda v_{x,\lambda}^2 c_\lambda\tau_\lambda \tag{20}$$

where V is the volume, $c_\lambda = \hbar\omega_\lambda\partial n_\lambda^0/\partial T$ is phonon specific heat per mode, and the summation is done over all the $3Nn_b$ modes with n_b representing the number of basis atoms in a primitive cell.

The formalism is applicable for one, two and three-dimensional crystals, and here we take graphene as an example for demonstration. The calculation for three-dimensional materials are more time-consuming.

The exact BTE solves all the phonons' scatterings simultaneously beyond the SMRTA. All the phonons are in their natural states, and their collective behavior is naturally captured. In SMRTA, a phonon mode is depopulated while all the final states are repopulated isothermally after a scattering process. Therefore, the phonons seem independent to each other. In contrast, in the exact BTE, each phonon's final state is coupled with all the other phonons' initial states. The results of former scattering events can affect the current scattering of all the other phonons. This can be seen from Eqs.(8)-(11), in which all the phonon modes are coupled with each other and the equations has to be solved via iteration. Especially when N process dominates (the momentum is conserved after scattering events), there are a large portion of phonon kicking each other to move forward continually. Such influence results in a collective motion of phonons, or so called relaxon[34]. We note that some interesting works have been done on the cross-correlation terms of the phonon normal modes in Green-Kubo method[35,36], and they can also determine the collective phonons' contribution. However, their method is different from the exact solution to BTE as the latter can separate clearly

the thermal conductivity contribution of each phonon branch while the former couples different modes' contributions together. Nevertheless, it is of great interest to further explore their relations.

III. CALCULATION DETAILS

The IFCs $\Phi^{\alpha\alpha'}_{0b,l'b'}$, $\Phi^{\alpha\alpha'\alpha''}_{0b,l'b',l''b''}$ and $\Phi^{\alpha\alpha'\alpha''\alpha'''}_{0b,l'b',l''b'',l'''b'''}$ are calculated by using the center finite difference method based on the optimized Tersoff potential [17], which has been shown to describe the anharmonic and other properties as accurately as DFT calculations for graphene [17]. In our work, the size of the **k**-mesh is 40×40. The lattice constant is taken as 2.492 $\AA$ [17]. The dispersion relation in high-symmetric directions (Γ-M-K) is shown in Fig. 1, which are identical to that given by Ref. [17].

Each fourth-order IFC (4-IFC) value requires double amount of computations of each third-order IFC (3-IFC). In Eqs. (17) and (18), the total required numbers of the 3-IFCs $\Phi^{\alpha\alpha'\alpha''}_{0b,l'b',l''b''}$ and 4-IFCs $\Phi^{\alpha\alpha'\alpha''\alpha'''}_{0b,l'b',l''b'',l'''b'''}$ are $27N^2n_b^3$ and $81N^3n_b^4$, respectively. $V^{(3)}_{\pm}$ and $V^{(4)}_{\pm\pm}$ are phonon mode dependent and have the dimensions of $3Nn_b$×$3Nn_b$ and $3Nn_b$×$3Nn_b$ ×$3Nn_b$, respectively. To sum up, the computational cost of the four-phonon scattering rate is about $9N^2n_b^2$ of the three-phonon scattering rate. In our work $N = 1600$, the required amount of memory and time in the calculation of the four-phonon scattering rate is about 9×10^7 times of the three-phonon scattering rate which seems impossible.

Several ways have been used to reduce the computational cost without losing accuracy. First, the IFC matrices contain a large number of zero elements which can be excluded in advance to reduce the computational cost. In our calculations, the ratios of the numbers of nonzero elements in the 3-IFC matrix and 4-IFC matrices are only about 10^{-7} and 10^{-11} respectively. Second, the IFC matrices are symmetric about the indices, i.e., $\Phi^{xyzx}_{1234} = \Phi^{xxyz}_{1423}$, which can further reduce the computational cost. This technique benefits the first principles approach more, where the calculation of the IFCs is the most time-consuming part. Third, in the calculations of $\mathcal{L}_{\pm}$ and $\mathcal{L}_{\pm\pm}$ in Eqs. (14,15), the computational cost can be largely reduced by excluding in advance the combinations that do not satisfy the MSR and ESR. For graphene, the computational cost can be further reduced by the reflection symmetry selection rule (RSSR), which is discussed in the following section. In addition, in the calculation of the relaxation times, the computation is reduced by about 3/4 by that fact that the **k** points in the first quadrant in the BZ have the same relaxation times with the other three quadrants.

Equation (2) is actually a system of $3Nn_b$ linear equations, which is solved by iterations. During the iteration the results can easily diverge[37]. In our work, we use the Gauss-Scidel method to do the iteration which is found to converge better and faster than the Jacobi method.

IV. RESULTS AND DISCUSSIONS

A. Reflection symmetry in three and four-phonon processes

For all the orders of phonon-phonon scattering, Lindsay *et al.* found that the RSSR in 2D materials forbids all the phonon-phonon scattering processes that involve an odd number of flexural (out-of-plane) modes [22]. Thus, the three-phonon processes may involve 0 or 2 flexural modes, while the four-phonon processes may involve 0, 2 or 4 flexural modes. Lindsay *et al.* has examined numerically that in graphene the three-phonon scattering rates of the processes that involve odd numbers of flexural modes are zeros [22]. In this work, we have verified numerically that such four-phonon scattering rates are zeros as well by the direct computation of Eq. (5).

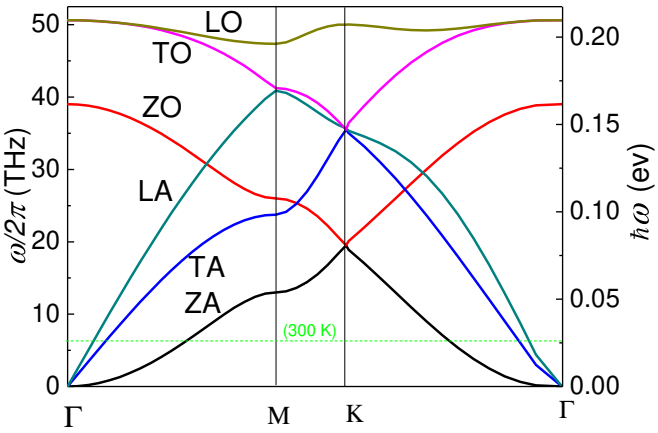

FIG. 1: The dispersion relation of graphene given by Eq. (19) using the optimized Tersoff potential. The green dashed line indicates that the thermal energy level at room temperature k_BT is not far above the energy $\hbar\omega$ of most phonons, and thus the classical quantities are not comparable to quantum quantities.

The RSSR is a unique property for 2D materials, and the study of how many scattering processes are forbidden by the RSSR is of great interest [22]. In Fig. 2, we show the percentage of the number of the processes that are forbidden purely by the RSSR, with MSR and ESR being already satisfied, as a function of the reduced wave vector (Γ-M). We find that most (60%-90%) of the three-phonon scattering processes of the ZA branch are forbidden by the RSSR, which allows ZA phonons high three-phonon relaxation times and a large contribution to the thermal conductivity as described in Ref. [22]. Compared to the three-phonon scattering, less (about 40%) four-phonon scattering processes of the ZA branch is forbidden by the RSSR, especially at low frequencies. This may result in a different conclusion to the relaxation time and the thermal conductivity contribution of the ZA phonons. Similar case is also observed for the TO and LO branches, e.g., 60%-90% of the three-phonon processes are forbidden while only 30%-40% for the four-phonon processes. Different trend is found in the TA and LA branches, in which more percentage of four-phonon processes is forbidden than the three-phonon

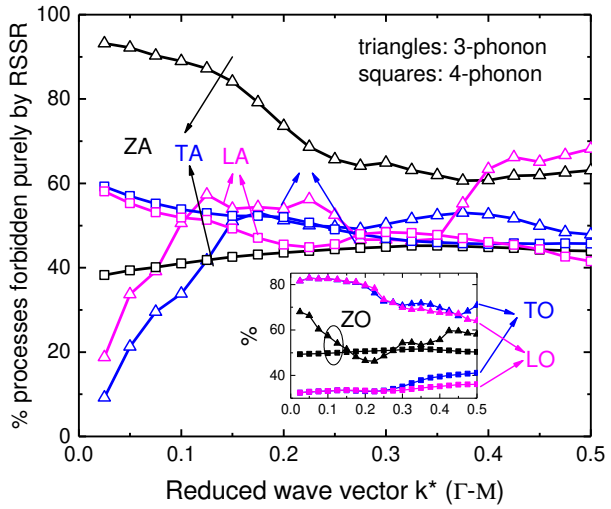

FIG. 2: The percentages of the numbers of processes that are purely forbidden by the RSSR. The main figure and the inset show the acoustic and the optical branches, respectively. Triangles represent three-phonon processes, and squres represent four-phonon processes.

TABLE I: The four-phonon scattering processes involving the ZA mode at $\mathbf{k}^*$=(0.25,0,0), which is labeled as ZA_0. Note that M point is at $\mathbf{k}^*$=(0.5,0,0). X stands for the modes other than the ZA branch, i.e., any combination of TA, LA, TO, LO, and ZO.

ZA_0	other 3 modes	available combinations	scattering rate
ZA_0+	3X	2630398	1.5×10^{-5} ps^{-1}
ZA_0+	ZA + 2X	6013776	7.6×10^{-4} ps^{-1}
ZA_0+	ZA + ZA + ZO	201815	4.6×10^{-5} ps^{-1}
ZA_0+	ZA + ZA + ZA	287777	0.487 ps^{-1}

processes at low frequencies. In addition, at the medium-to-high frequencies, the three-phonon scattering and four-phonon scattering are generally forbidden by 50-70% and 35%-50%, respectively, for all the six branches.

B. High four-phonon scattering rates based on SMRTA

The room-temperature three- and four-phonon scattering rates, $(\tau^0_{3,\lambda})^{-1}$ and $(\tau^0_{4,\lambda})^{-1}$, as a function of reduced wave vector from Γ to M are shown in Fig. 3 (a). Astonishingly, we find that the four-phonon rates are comparable to or even much higher than the three-phonon rates, even at room temperature, especially for the ZA, TO and LO branches. For instance, the three-phonon rates of the ZA branch are typically below 0.08 ps^{-1} while the four-phonon rates are about 0.42-2 ps^{-1}, which indicates the relaxation time of ZA mode at room temperature is about 0.5-2 ps, far below expectation. Both N and U processes are found to follow the temperature dependence of $(\tau^0_{3,\lambda})^{-1} \sim T$ and $(\tau^0_{3,\lambda})^{-1} \sim T^2$, not shown here[26,27]. Those temperature dependences indicate that the four-phonon processes play a more important role at higher temperatures. At 700 K, the four-phonon rates of the ZA, TO and LO branches

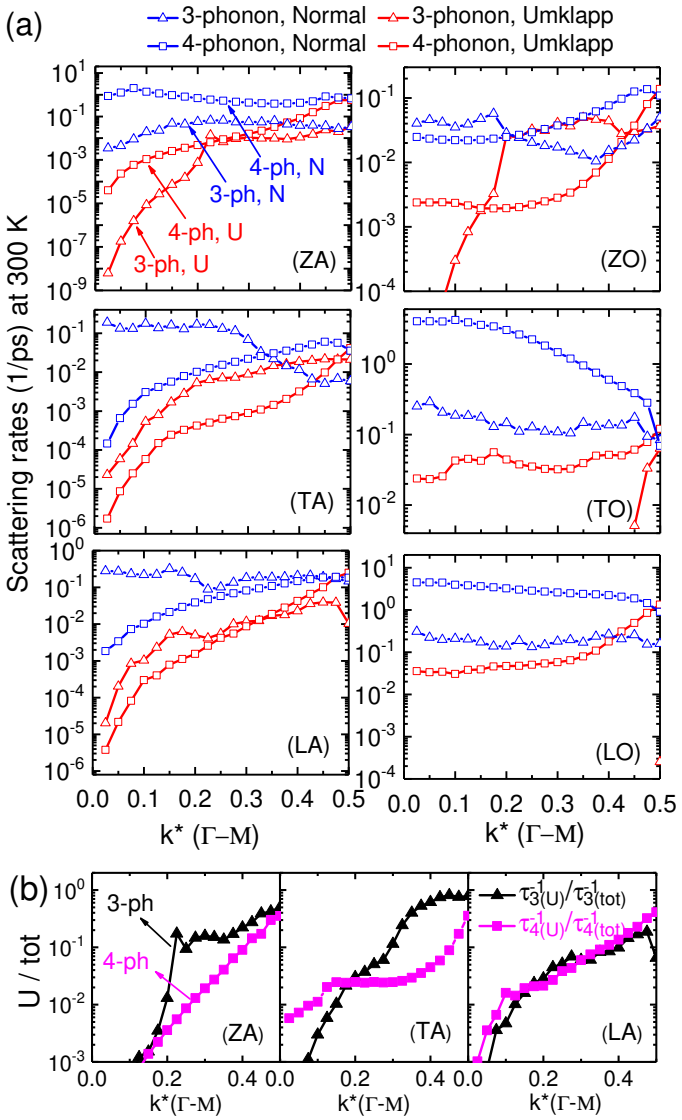

FIG. 3: (a) The three-phonon and four-phonon scattering rates, $\tau^{-1}_{3(N)}$, $\tau^{-1}_{3(U)}$, $\tau^{-1}_{4(N)}$ and $\tau^{-1}_{4(U)}$ of the six branches with respect to the reduced wave vector (Γ-M) at 300 K. (b) The weights of U processes for the three acoustic branches: $\tau^{-1}_{3(U)}/\tau^{-1}_{3(tot)}$ [black solid triangles], $\tau^{-1}_{4(U)}/\tau^{-1}_{4(tot)}$ [pink solid squares].

reach even above 10 ps^{-1}, being 2-3 orders higher than the three-phonon rates. Those results break the general rule in bulk materials that four-phonon scattering is more important in more strongly anharmonic materials [26,27], while graphene is a relatively strongly harmonic material. Such a phenomenon indicates a significant difference between 2D and bulk materials. We note that the branches (ZA, TO and LO) that have extraordinarily high four-phonon rates are those that are forbidden relatively fewer four-phonon than three-phonon processes by the RSSR as shown in Fig. 2.

To look into the reason for the high four-phonon scattering rate in computational aspect, we find that although the probability of each four-phonon scattering process is extremely low,

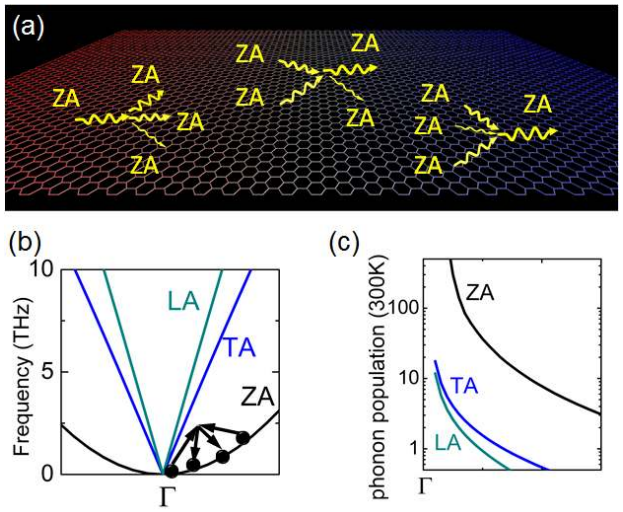

FIG. 4: Collective four-phonon transport in graphene. (c) The population of the ZA phonons is significantly higher than the other phonons, especially in the low-frequency region.

the phase space allows a great number of such processes to happen. Specifically, for each phonon mode the three selection rules allow about $\sim 10^2$ numbers of three-phonon processes while allow about $10^6 - 10^7$ four-phonon processes.

To gain physical insights into the ultra-high four-phonon scattering rates of the ZA mode, we have looked into the detailed scattering processes involving it. Taking the ZA mode at $\mathbf{k}^*$=(0.25,0,0), the middle point of ΓM, labeled as ZA_0, as an example, we investigate the scattering rates of all the possible four-phonon processes as shown in Table I. The processes are divided into four categories determined by the number of other ZA phonons involved. For each category, the number of available four-phonon combinations is considerably large. Surprisingly, only the category ZA_0+ZA+ZA+ZA has a visible scattering rate, which includes ZA_0→ZA+ZA+ZA, ZA_0+ZA→ZA+ZA, and ZA_0+ZA+ZA→ZA. This finding indicates that the transport of ZA phonons is dominated by the four-ZA processes, as shown in Fig.4. Since ZA phonons have much larger population than the other modes as shown in Fig.4 (c) and the four-phonon scattering rate is proportional to the square of the population, the four-ZA process has much larger scattering rate than the other processes. In contrast, the three-phonon process cannot involve three ZA modes due to the reflection symmetry, and the three-phonon scattering rate is only linear to the population, therefore the τ_3^{-1} of ZA phonons is low. Since most of four-phonon processes are *N* processes as discussed in the following text, these four-ZA processes lead to an collective phonon transport with an hydrodynamical behavior [38,39]. An earlier work based on molecular dynamics has found evidence of the importance of the higher-order scattering in graphene [18], which strongly supports our results.

C. Dominant *N* processes in four-phonon scattering

As suggested by Ref. [22], for materials such as graphene in which the *N* process dominates three-phonon scattering, an iterative method is required to exclude the *N* process in calculating the phonon relaxation time. Thus, it is necessary to examine whether the *N* process dominates the four-phonon scattering. In Fig. 3 (a), it is clearly seen that the *N* process dominates the four-phonon scattering. In Fig. 3 (b), we show the ratios of the *U* scattering rates to the total scattering rates, $(\tau^0_{3,U})^{-1}/(\tau^0_3)^{-1}$ and $(\tau^0_{4,U})^{-1}/(\tau^0_4)^{-1}$, with respect to the reduced wave vector in the six branches at 300 K. Both ratios increase with increasing reduced wave vector since the scattering of large wave vectors is more likely to reach out of the first BZ. In comparison, $(\tau^0_{4,U})^{-1}/(\tau^0_4)^{-1}$ in graphene is much lower than $(\tau^0_{3,U})^{-1}/(\tau^0_3)^{-1}$, giving a distinct contrast to the bulk materials in which the *U* process typically dominates the four-phonon scattering [26,27]. Specifically, $(\tau^0_{4,U})^{-1}/(\tau^0_4)^{-1}$ is nearly zero throughout a broad wave vector range and has a modest increase near the BZ boundary. As temperature increases, the portion of Normal process in four-phonon scattering does not decrease much, although the one in three-phonon scattering decreases, not shown here. Therefore, the exact solution to BTE that involves the four-phonon processes is required at all temperatures.

Since the *U* processes directly contribute to the thermal resistance, it is necessary to compare the *U* rates between the four-phonon and three-phonon scatterings. As seen in Fig. 3 (a), $\tau^{-1}_{4,U}$ is much higher than $\tau^{-1}_{3,U}$ for the ZA, TO and LO modes, and lower for other modes. Therefore, it is expected that the four-phonon scattering can substantially reduce the thermal conductivities of the ZA, TO and LO branches.

D. Thermal conductivity reduction due to four-phonon scattering

With the SMRTA scattering rates, we exactly solve the linearized phonon BTE using an iterative scheme. In Fig. 5, we show the thermal conductivities κ_3 and κ_{34} of 9-μm graphene at room temperature as a function of the iteration step. κ_3 is calculated by including the three-phonon scattering only, and κ_{34} includes both the three and four-phonon scatterings. The iterations typically converge after 5-10 steps when four-phonon is included, and such a fast speed results from the Gauss-Scidel iteration algorithm. The convergence speed slows down when the length of the graphene increases, due to the decreases of the boundary scattering, not shown here. The iterations significantly increase the predicted thermal conductivity values for all branches. Our result of $\kappa_{3,ZA}$ agrees well with the ~ 2260 W/mK given by Lindsay et al [22]. In Fig. 5 (b), the ZA branch has the most growth among the acoustic branches with regard to the iteration step. By comparing Fig. 5 (a) and (b), we find that the thermal conductivity of 9-μm graphene is reduced significantly from ~3383 W/mK to ~810 W/mK after including the four-phonon scattering. This reduction mainly comes from the ZA branch, whose thermal conductivity is reduced from

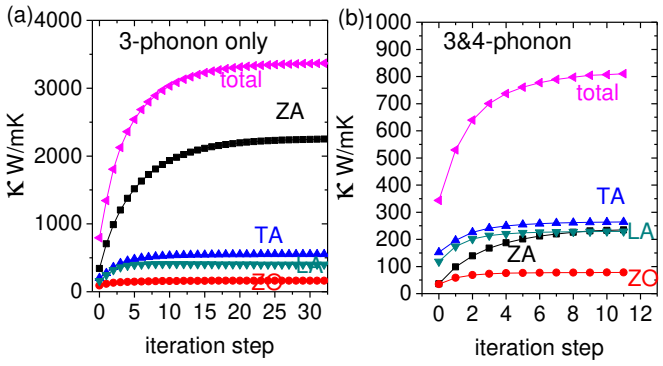

FIG. 5: The predicted thermal conductivities of 9-μm graphene at room temperature as a function of iteration step using the Optimized Tersoff potential. The SMRTA results are at the iteration step = 0.

$\kappa_{3,ZA}$ ~2260 W/mK to $\kappa_{34,ZA}$ ~235 W/mK.

The length-dependent thermal conductivities of graphene at room temperature predicted by different methods are summarized in Figs.6 (a) and (b). We only show the results from the optimized Tersoff potential and first principles (FP) since the other potentials do not present an accurate phonon dispersion relation [2,22]. It is seen that our three-phonon thermal conductivity κ_3 agrees well with the results from literatures. The inclusion of four-phonon scattering reduces the thermal conductivity substantially. Both of them converges well with length, with the former converging starting from ~ 100 μm and the latter ~ 10 μm. The converged values are about 4285 W/mK and 850 W/mK, respectively. Since the fourth-order force constant of the classical interatomic potential has not been validated against first principles[17], the absolute values of the thermal conductivity after including four-phonon scattering should be interpreted qualitatively.

To compare with experiment, we plot the temperature-dependent thermal conductivity of graphene in Fig. 6 (c). The large uncertainty of the experimental measurement makes it hard to validate the predictions from literatures and this work. Raman technique[4,7,8,12–14,44,45] [open triangles] generally gives higher thermal conductivity than the other experimental methods[8,42,43] [solid triangles]. We note that a work has pointed out that the thermal conductivity measurement of graphene by Raman technique is not reliable[46]. If we compare the other measurements with the theoretical prediction, the κ_{34} agrees better than κ_3. Nevertheless, the agreement is only within the same order especially at low temperature. The experimental data at low temperatures are quite low, possibly due to 1) the contact thermal resistance was assumed to be temperature-independent in the experiments and 2) the possible defects and grain boundaries in experimental samples affect thermal conductivities at low temperatures more than at high temperatures since the phonon-phonon scatterings at low temperatures are weak. To have a better comparison, both experiment and theoretical prediction need to be improved. On the experimental side, the single-crystal single layer graphene sample requires high quality with negligible defects, boundaries or chemical residues, and a reliable method of excluding the contact resistance needs to be developed. On the theoretical

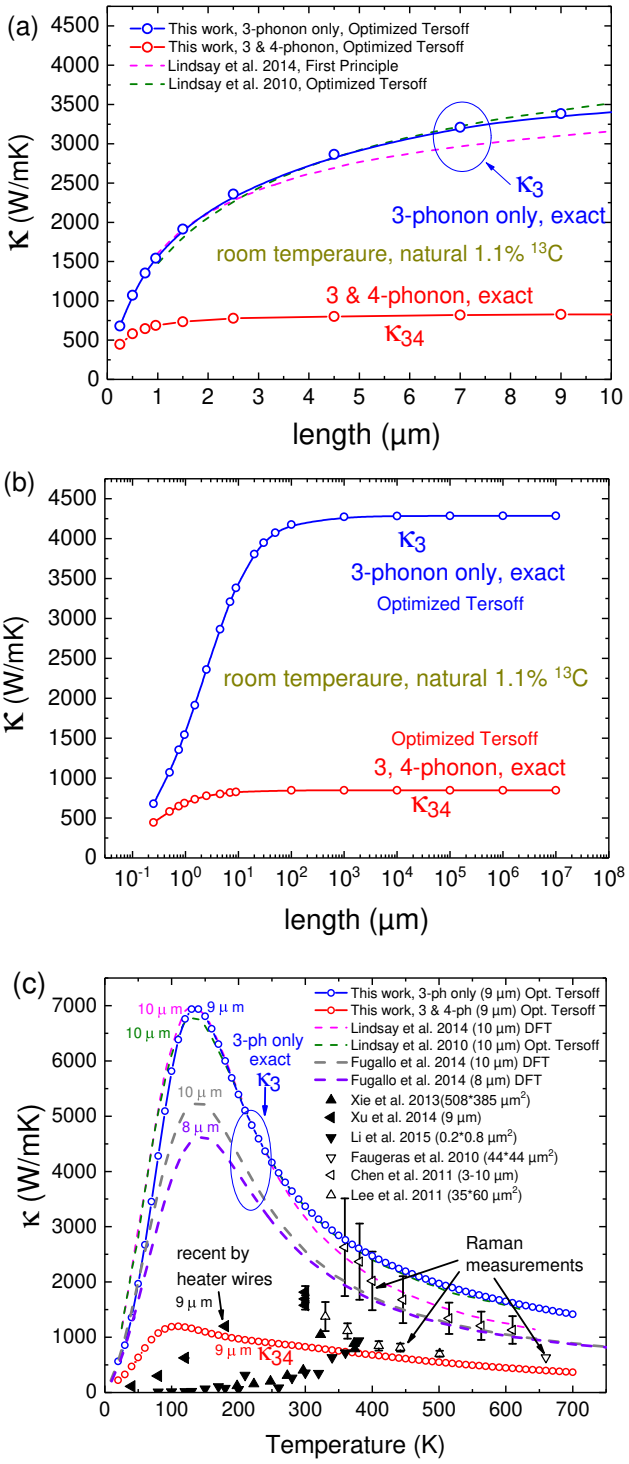

FIG. 6: (a) Length-dependent thermal conductivity of single-layer graphene at 300 K. (b) Length convergence of thermal conductivity at 300 K. (c) Temperature-dependent lattice thermal conductivity. The dash lines represent the theoretical predictions from the literature with three-phonon scattering only. The solid lines with open circles represent the predictions from this work. In all the predictions, the natural 1.1% ^{13}C is included with the exact solution to the linearized BTE. The triangles shown the experimental measured results. References: Lindsay et al. [22,40], Fugallo et al. [41], Xie et al. [42], Xu et al. [8], Li et al. [43], Faugeras et al. [12], Chen et al. [44], Lee et al. [45].

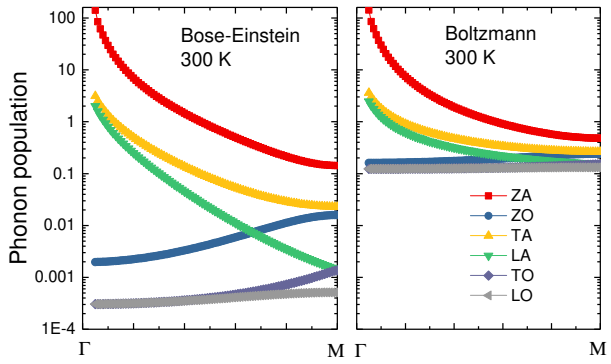

FIG. 7: The phonon population of SLG calculated via Bose-Einstein and Boltzmann distributions at 300 K.

side, the fourth order interatomic force constants obtained from the Optimized Tersoff potential need to be validated against first principles based on density functional theory. These are beyond our scope, but certainly worth to investigate.

We note that the thermal conductivity of SLG calculated by Gill-Comeau and Lewis [35,36] and Fan *et al.* [47,48] recently by the optimized Tersoff potential using MD simulations is about 2000-3000 W/mK, which is much higher than the present BTE results with four-phonon scattering included. We attribute the difference to the usage of different phonon distribution functions. As shown in Fig.7, the phonon populations differ significantly between the two distributions. We note that some quantum corrections [18,25,35,36] have been made to correct the difference in specific heat, however, the impact on phonon scattering was not included. As the scattering rates depend strongly on phonon population, we expect the two distributions give significantly different phonon scattering rates. To probe such an effect, some work [49] has used the Boltzmann distribution in the three-phonon scattering formalism to calculate the phonon scattering rates. However, as a previous work[26] has proved, the three-phonon (and four-phonon) scattering formalism is only valid for the Bose-Einstein distribution as its derivation depends on the Bose-Einstein distribution. It is unreasonable to use Boltzmann distribution in a formula that is derived only for Bose-Einstein distribution, especially at low temperatures. Also, it is unreasonble to conclude from Fig.7 that the Boltzmann distribution gives more scattering due to the larger phonon population since the scattering formalism itself is not valid.

E. Thermal conductivity contribution from each branch

The relative κ contributions from different branches predicted by the three and four-phonon scatterings are compared in Table II. It has long been in debate which branch dominates the thermal transport, with the detailed discussion found in the review[2]. The relative contribution of the ZA branch is reduced from 60% to 30% after including four-phonon scattering. The

TABLE II: The comparison among the different methods on the predicted relative contribution from individual branch to κ of SLG at room temperature. The results from equilibrium MD (EMD) and non-equilibrium MD (NEMD) from Ref.a[48] are included.

κ%	3-phonon only		3, 4-phonon		EMD		NEMD
	SMRTA	Exact BTE	SMRTA	Exact BTE	NMA	Green-Kubo[a]	Decom-position[a]
ZA%	52%	60%	17%	31%	30%	71%	52%
ZO%	8%	4%	11%	8%	7%		
TA%	22%	20%	41%	32%	27%	29%	48%
LA%	17%	16%	31%	28%	35%		

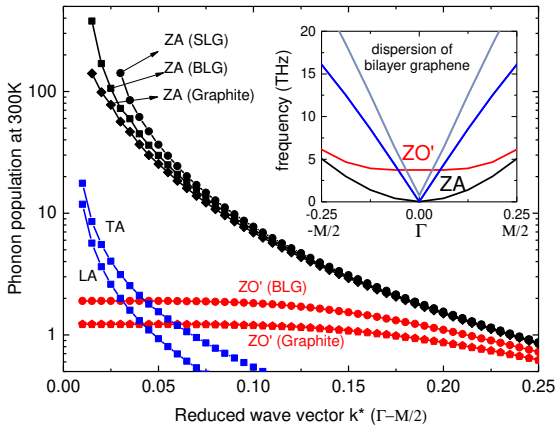

FIG. 8: The phonon population in bilayer graphene (BLG) and graphite. Inset shows the ZA splitting in bilayer graphene (similarly in graphite). Phonon dispersion is calculated from the intra-layer optimized Tersoff potential together with the interlayer Lennard-Jones potential with parameters same as Ref.[50].

contribution of TA and LA branches increase to around 30%. These results are compared to those from MD simulations. We note that different MD simulations give substantially different interpretations for the branch contributions. Nevertheless, as being stated above, MD simulations assume the Boltzmann distribution which may significantly vary the phonon scattering mechanisms, and thus the comparison between BTE and MD should not be taken seriously at temperatures below the Debye temperature.

F. More discussions

Since we have found the ultra-high four-phonon scattering rates in SLG, two natural questions are: 1) Does the four-phonon scattering play an important role in multilayer graphene and graphite? 2) Is the five-phonon scattering important in SLG? To address the first question, we plot the phonon dispersion in the inset of Fig. 8. Due to the interlayer van der Waals interaction, the ZA mode of graphene is spitted into the ZA and ZO′ modes, with the latter representing a breathing mode between adjacent layers. We find that even such a small spitting can result in a large reduction of the phonon popula-

tion as shown in Fig. 8. Due to the splitting, the phase space of the four-ZA process becomes 1/16 of the SLG, and thus the four-phonon scattering becomes unimportant. This explains the fact that the three-phonon thermal conductivity prediction of graphite agrees well with experiment[41,50]. Regarding the second question, we need to refer to the reflection symmetry. Restricted by the ASSR, the five-phonon process can at most involve four ZA modes, same as four-phonon scattering. Without increasing the population, the higher order makes the five-phonon scattering negligible.

V. CONCLUSIONS

We have shown that the four-phonon scattering formalism can be incorporated into the exact solution to BTE. We take graphene as an example to demonstrate our method and have obtained well-converged results. We find that the four-phonon scattering rate in graphene is surprisingly high due to the fact that the reflection symmetry allows significantly more four-phonon processes than three-phonon processes. In particular, the allowed four-ZA processes together with the quadratic phonon dispersion push the four-phonon rates of the ZA branch to an unprecedented level. Since these scatterings are dominated by the Normal processes, the exact solution to BTE is required beyond the single mode relaxation time approximation. We find that the thermal conductivity of graphene is significantly reduced when the four-phonon scattering is included. We expect such high four-phonon scattering rates also exist in single layer BN and other possible planar 2D materials, which have similar phonon dispersion and reflection symmetry with SLG. To have a rational comparison with experiment, more accurate experimental measurements and accurate DFT force constants are required. Our work advances the thermal transport calculation by incorporating four-phonon scattering into the exact solution to BTE. Our finding is striking in the thermal transport in 2D materials with reflection symmetry, and provides a critical revisit to the exact thermal conductivity value of single-layer graphene.

Acknowledgments

Simulations were performed at the Rosen Center of Advanced Computing at Purdue University. The work was partially supported by the National Science Foundation (Award No. 1150948).

Appendix A: Derivation of the Solution to linearized phonon BTE

Starting from Eq. (1), due to a small temperature gradient, n_λ has a small derivation n'_λ from its equilibrium Bose-Einstein distribution $n^0_\lambda = [\exp(\hbar\omega_\lambda/k_BT) - 1]^{-1}$ so that $n_\lambda = n^0_\lambda + n'_\lambda$. By assuming that n'_λ is independent of temperature[30]: $(\partial n_\lambda/\partial T) \simeq (\partial n^0_\lambda/\partial T)$, we have

$$\mathbf{v}_\lambda \cdot \nabla T \frac{\partial n^0_\lambda}{\partial T} = \frac{\partial n'_\lambda}{\partial t}|_s, \tag{A1}$$

with the help of $\nabla n_\lambda = (\partial n_\lambda/\partial T)\nabla T$. The scattering term $\frac{\partial n'_\lambda}{\partial t}|_s$ is the decay rate of the perturbation n'_λ due to the scattering processes, such as phonon-phonon, phonon-impurity, and phonon-boundary scattering.

Based on the perturbation theory, the right hand side of Eq. (A1) is rewritten as, considering the three-phonon[16,29–31,51], four-phonon[26], isotope[52] and boundary[53–55] scattering,

$$\begin{aligned}\frac{\partial n'_\lambda}{\partial t}|_s = & -\sum_{\lambda'\lambda''}\left\{\frac{1}{2}\left[n_\lambda(1+n_{\lambda'})(1+n_{\lambda''})-(1+n_\lambda)n_{\lambda'}n_{\lambda''}\right]\mathcal{L}_- + \left[n_\lambda n_{\lambda'}(1+n_{\lambda''})-(1+n_\lambda)(1+n_{\lambda'})n_{\lambda''}\right]\mathcal{L}_+\right\} \\ & -\sum_{\lambda'\lambda''\lambda'''}\left\{\frac{1}{6}\left[n_\lambda(1+n_{\lambda'})(1+n_{\lambda''})(1+n_{\lambda'''})-(1+n_\lambda)n_{\lambda'}n_{\lambda''}n_{\lambda'''}\right]\mathcal{L}_{--} + \frac{1}{2}\left[n_\lambda n_{\lambda'}(1+n_{\lambda''})(1+n_{\lambda'''})-(1+n_\lambda)(1+n_{\lambda'})n_{\lambda''}n_{\lambda'''}\right]\mathcal{L}_{+-}\right. \\ & \left. +\frac{1}{2}\left[n_\lambda n_{\lambda'}n_{\lambda''}(1+n_{\lambda'''})-(1+n_\lambda)(1+n_{\lambda'})(1+n_{\lambda''})n_{\lambda'''}\right]\mathcal{L}_{++}\right\} - \sum_{\lambda''}(n_\lambda - n_{\lambda''})\mathcal{L}_{iso} - (n_\lambda - n^0_\lambda)\frac{1}{\tau^0_{b,\lambda}}.\end{aligned} \tag{A2}$$

The first summation on the right hand side represents the three-phonon scattering rate of the mode λ, with the first term accounting for the splitting process $\lambda \to \lambda' + \lambda''$ and the second the combination process $\lambda + \lambda' \to \lambda''$. The physical meaning of the first term is the difference between the transition probabilities of $\lambda \to \lambda' + \lambda''$ and $\lambda \leftarrow \lambda' + \lambda''$, and thus indicates the net decay rate of n_λ due to the splitting process. Similarly, the second term illustrates the transition probability difference between $\lambda + \lambda' \to \lambda''$ and $\lambda + \lambda' \leftarrow \lambda''$, indicating the net decay rate of n_λ due to the combination process. $\mathcal{L}_\pm$ contains the information of the intrinsic transition probability and the transition selection rules for energy and momentum, $\omega_\lambda \pm \omega_{\lambda'} - \omega_{\lambda''} = 0$ and $\mathbf{k} \pm \mathbf{k}' - \mathbf{k}'' = \mathbf{G}$, where $\mathbf{G}$ is a reciprocal lattice vector with $\mathbf{G} = 0$ implying the Normal (N) process and $\mathbf{G} \neq 0$ the Umklapp (U) process. The second summation accounts for the four-phonon scattering of the

mode λ, with the first parentheses representing the process $\lambda \rightarrow \lambda' + \lambda'' + \lambda'''$, the second the process $\lambda + \lambda' \rightarrow \lambda'' + \lambda'''$ and the third $\lambda + \lambda' + \lambda'' \rightarrow \lambda'''$. Similarly, $\mathcal{L}_{\pm\pm}$ accounts for the transition probabilities and the selection rules, i.e., $\omega_\lambda \pm \omega_{\lambda'} \pm \omega_{\lambda''} - \omega_{\lambda'''} = 0$ and $\mathbf{k} \pm \mathbf{k}' \pm \mathbf{k}'' - \mathbf{k}''' = \mathbf{G}$, for those processes. The third summation is the phonon-isotope scattering rate for $\lambda \rightarrow \lambda'$ given by Tamura [52], with the selection rules $\omega_\lambda = \omega_{\lambda'}$ and $\mathbf{k} \neq \mathbf{k}'$. The last term on the right hand side of Eq. (A2) indicates the phonon-boundary scattering rate. The minus sign before each scattering term indicates that the perturbation n'_λ is decreasing with time, i.e., the phonon distribution tends to recover its equilibrium state, due to the scattering. In contrast to the SMRTA [16,30], which assumes that only the mode λ has a perturbation, here we assumes a perturbation in all the phonon modes to exactly solve the phonon BTE [28,29,33,56], that is

$$n_\lambda = n^0_\lambda + n'_\lambda, n'_\lambda = -\Psi_\lambda \frac{\partial n^0_\lambda}{\partial(\hbar\omega_\lambda)} = \Psi_\lambda \cdot \frac{1}{k_B T} n^0_\lambda (n^0_\lambda + 1), \tag{A3}$$

$$n_{\lambda'} = n^0_{\lambda'} + n'_{\lambda'}, n'_{\lambda'} = -\Psi_{\lambda'} \frac{\partial n^0_{\lambda'}}{\partial(\hbar\omega_{\lambda'})} = \Psi_{\lambda'} \cdot \frac{1}{k_B T} n^0_{\lambda'} (n^0_{\lambda'} + 1), \tag{A4}$$

$$n_{\lambda''} = n^0_{\lambda''} + n'_{\lambda''}, n'_{\lambda''} = -\Psi_{\lambda''} \frac{\partial n^0_{\lambda''}}{\partial(\hbar\omega_{\lambda''})} = \Psi_{\lambda''} \cdot \frac{1}{k_B T} n^0_{\lambda''} (n^0_{\lambda''} + 1), \tag{A5}$$

$$n_{\lambda'''} = n^0_{\lambda'''} + n'_{\lambda'''}, n'_{\lambda'''} = -\Psi_{\lambda'''} \frac{\partial n^0_{\lambda'''}}{\partial(\hbar\omega_{\lambda'''})} = \Psi_{\lambda'''} \cdot \frac{1}{k_B T} n^0_{\lambda'''} (n^0_{\lambda'''} + 1), \tag{A6}$$

where Ψ measures the derivation in the phonon distribution from equilibrium, weighted with a factor that depends on the equilibrium distribution of that mode [29]. In the final step of each of the Eqs. (A3-A6), we used the fact that $\partial n^0/\partial(\hbar\omega) = -n^0(n^0+1)/k_B T$. By substituting Eqs. (A3-A6) into Eq. (A2) and dropping the higher order terms $O(\Psi^2)$ and $O(\Psi^3)$, the scattering term of the linearized phonon BTE is written as

$$\begin{aligned}
\frac{\partial n'_\lambda}{\partial t}|_s = & -\sum_{\lambda'\lambda''} \frac{1}{k_B T} \left\{ (\Psi_\lambda + \Psi_{\lambda'} - \Psi_{\lambda''}) n^0_\lambda n^0_{\lambda'} (1 + n^0_{\lambda''}) \mathcal{L}_+ + \frac{1}{2} (\Psi_\lambda - \Psi_{\lambda'} - \Psi_{\lambda''}) n^0_\lambda (1 + n^0_{\lambda'}) (1 + n^0_{\lambda''}) \mathcal{L}_- \right\} \\
& - \sum_{\lambda'\lambda''\lambda'''} \frac{1}{k_B T} \left\{ \frac{1}{6} (\Psi_\lambda - \Psi_{\lambda'} - \Psi_{\lambda''} - \Psi_{\lambda'''}) (1 + n^0_\lambda) n^0_{\lambda'} n^0_{\lambda''} n^0_{\lambda'''} \mathcal{L}_{--} + \frac{1}{2} (\Psi_\lambda + \Psi_{\lambda'} - \Psi_{\lambda''} - \Psi_{\lambda'''}) (1 + n^0_\lambda) n^0_{\lambda'} n^0_{\lambda''} n^0_{\lambda'''} \mathcal{L}_{+-} \right. \\
& \left. + \frac{1}{2} (\Psi_\lambda + \Psi_{\lambda'} + \Psi_{\lambda''} - \Psi_{\lambda'''}) (1 + n^0_\lambda) (1 + n^0_{\lambda'}) (1 + n^0_{\lambda''}) n^0_{\lambda'''} \mathcal{L}_{++} \right\} \\
& - \sum_{\lambda'} \frac{1}{k_B T} (\Psi_\lambda - \Psi_{\lambda'}) n^0_\lambda (1 + n^0_\lambda) \mathcal{L}_{iso} - \frac{1}{k_B T} \Psi_\lambda n^0_\lambda (1 + n^0_\lambda) \frac{1}{\tau^0_{b,\lambda}}.
\end{aligned} \tag{A7}$$

Here we have taken the advantage of the facts:

$$\lambda \rightarrow \lambda' + \lambda'' : (1+n^0_{\lambda'})(1+n^0_{\lambda''}) - n^0_{\lambda'} n^0_{\lambda''} = \frac{n^0_{\lambda'} n^0_{\lambda''}}{n^0_\lambda} = 1 + n^0_{\lambda'} + n^0_{\lambda''}, \tag{A8}$$

$$\lambda + \lambda' \rightarrow \lambda'' : n^0_{\lambda'}(1+n^0_{\lambda''}) - (1+n^0_{\lambda'}) n^0_{\lambda''} = \frac{(1+n^0_{\lambda'}) n^0_{\lambda''}}{n^0_\lambda} = n^0_{\lambda'} - n^0_{\lambda''}, \tag{A9}$$

$$\lambda \rightarrow \lambda' + \lambda'' + \lambda''' : (1+n^0_{\lambda'})(1+n^0_{\lambda''})(1+n^0_{\lambda'''}) - n^0_{\lambda'} n^0_{\lambda''} n^0_{\lambda'''} = \frac{n^0_{\lambda'} n^0_{\lambda''} n^0_{\lambda'''}}{n^0_\lambda}, \tag{A10}$$

$$\lambda + \lambda' \rightarrow \lambda'' + \lambda''' : n^0_{\lambda'}(1+n^0_{\lambda''})(1+n^0_{\lambda'''}) - (1+n^0_{\lambda'}) n^0_{\lambda''} n^0_{\lambda'''} = \frac{(1+n^0_{\lambda'}) n^0_{\lambda''} n^0_{\lambda'''}}{n^0_\lambda}, \tag{A11}$$

$$\lambda + \lambda' + \lambda'' \rightarrow \lambda''' : n^0_{\lambda'} n^0_{\lambda''}(1+n^0_{\lambda'''}) - (1+n^0_{\lambda'})(1+n^0_{\lambda''}) n^0_{\lambda'''} = \frac{(1+n^0_{\lambda'})(1+n^0_{\lambda''}) n^0_{\lambda'''}}{n^0_\lambda}. \tag{A12}$$

Equations (A8-A12) are obtained in similar way. For example, Equation (A8) is derived by substituting the ω of the Bose-Einstein distribution $e^{\hbar\omega/k_BT} = 1 + 1/n^0_\lambda$ into the energy conservation law (selection rule) $\omega = \omega' + \omega''$, giving the result $1 + 1/n^0_\lambda = (1 + 1/n^0_{\lambda'})(1 + 1/n^0_{\lambda''})$.

The final expression of the right hand side of the original phonon BTE Eq. (A1) is obtained by defining the form [33] of $\Psi = -h\omega\tau\mathbf{v}\cdot\nabla T/T$ and putting it into Eq. (A7) for all the modes λ, λ', λ'', and λ''', while the left hand side of Eq. (A1) is transformed by the fact of

$$\frac{\partial n^0_\lambda}{\partial T} = \frac{1}{T}\frac{\hbar\omega_\lambda}{k_BT} n^0_\lambda (n^0_\lambda + 1). \tag{A13}$$

Thus, the phonon BTE Eq. (A1) is transformed as

$$\begin{aligned} 1 = & \sum_{\lambda'\lambda''} \left\{ (\tau_\lambda + \tau_{\lambda'}\xi_{\lambda\lambda'} - \tau_{\lambda''}\xi_{\lambda\lambda''}) \frac{n^0_{\lambda'}(1+n^0_{\lambda''})}{1+n^0_\lambda} \mathcal{L}_+ + \frac{1}{2}(\tau_\lambda - \tau_{\lambda'}\xi_{\lambda\lambda'} - \tau_{\lambda''}\xi_{\lambda\lambda''}) \frac{n^0_{\lambda'}(1+n^0_{\lambda''})}{1+n^0_\lambda} \mathcal{L}_- \right\} \\ & + \sum_{\lambda'\lambda''\lambda'''} \left\{ \frac{1}{6}(\tau_\lambda - \tau_{\lambda'}\xi_{\lambda\lambda'} - \tau_{\lambda''}\xi_{\lambda\lambda''} - \tau_{\lambda'''}\xi_{\lambda\lambda'''}) \frac{n^0_{\lambda'} n^0_{\lambda''} n^0_{\lambda'''}}{n^0_\lambda} \mathcal{L}_{--} + \frac{1}{2}(\tau_\lambda + \tau_{\lambda'}\xi_{\lambda\lambda'} - \tau_{\lambda''}\xi_{\lambda\lambda''} - \tau_{\lambda'''}\xi_{\lambda\lambda'''}) \frac{(1+n^0_{\lambda'}) n^0_{\lambda''} n^0_{\lambda'''}}{n^0_\lambda} \mathcal{L}_{+-} \right. \\ & \left. + \frac{1}{2}(\tau_\lambda + \tau_{\lambda'}\xi_{\lambda\lambda'} + \tau_{\lambda''}\xi_{\lambda\lambda''} - \tau_{\lambda'''}\xi_{\lambda\lambda'''}) \frac{(1+n^0_{\lambda'})(1+n^0_{\lambda''}) n^0_{\lambda'''}}{n^0_\lambda} \mathcal{L}_{++} \right\} + \sum_{\lambda'} (\tau_\lambda - \tau_{\lambda'}\xi_{\lambda\lambda'}) \mathcal{L}_{iso} + \frac{\tau_\lambda}{\tau^0_{b,\lambda}}, \end{aligned} \tag{A14}$$

and further as

$$1 = \frac{\tau_\lambda}{\tau^0_{3,\lambda}} - \Xi_{3,\lambda} + \frac{\tau_\lambda}{\tau^0_{4,\lambda}} - \Xi_{4,\lambda} + \frac{\tau_\lambda}{\tau^0_{iso,\lambda}} - \Xi_{iso,\lambda} + \frac{\tau_\lambda}{\tau^0_{b,\lambda}}. \tag{A15}$$

Then, the solution of τ_λ is obtained as shown in Eq. (2), with the sub-equations (3-18). Substituting τ_λ into Eq. (A3), the solution of the linearized phonon BTE is expressed as

$$n_\lambda = n^0_\lambda - \frac{\hbar\omega_\lambda}{k_BT} n^0_\lambda (n^0_\lambda + 1) \frac{\mathbf{v}_\lambda \cdot \nabla T}{T} \tau_\lambda. \tag{A16}$$

Appendix B: Hamiltonians for three-phonon, four-phonon and isotope scattering

The start point of the derivation of the transition probabilities is the Hamiltonian of the solids [51,52]

$$\begin{aligned} \hat{H} &= \hat{H}_0 + \hat{H}_a + \hat{H}_{iso} + \cdots \\ &= \hat{H}_0 + \hat{H}_3 + \hat{H}_4 + \cdots + \hat{H}_{iso} + \cdots, \end{aligned} \tag{B1}$$

where

$$\hat{H}_0 = \sum_{\lambda} \hbar\omega_\lambda (a^\dagger_\lambda a_\lambda + 1/2), \tag{B2}$$

$$\hat{H}_3 = \sum_{\lambda\lambda'\lambda''} H^{(3)}_{\lambda\lambda'\lambda''} (a^\dagger_{-\lambda} + a_\lambda)(a^\dagger_{-\lambda'} + a_{\lambda'})(a^\dagger_{-\lambda''} + a_{\lambda''}), \tag{B3}$$

$$\hat{H}_4 = \sum_{\lambda\lambda'\lambda''\lambda'''} H^{(4)}_{\lambda\lambda'\lambda''\lambda'''} (a^\dagger_{-\lambda} + a_\lambda)(a^\dagger_{-\lambda'} + a_{\lambda'})(a^\dagger_{-\lambda''} + a_{\lambda''})(a^\dagger_{-\lambda'''} + a_{\lambda'''}), \tag{B4}$$

$$\hat{H}_{iso} = \sum_{\lambda\lambda'} H^{(iso)}_{\lambda\lambda'} (a^\dagger_{-\lambda} + a_\lambda)(a^\dagger_{-\lambda'} + a_{\lambda'}), \tag{B5}$$

$$H^{(3)}_{\lambda\lambda'\lambda''} = \frac{\hbar^{3/2}}{2^{3/2} \times 6N^{1/2}} \Delta_{\mathbf{k}+\mathbf{k}'+\mathbf{k}'',\mathbf{G}} \frac{V^{(3)}_{\lambda\lambda'\lambda''}}{\sqrt{\omega_\lambda \omega_{\lambda'} \omega_{\lambda''}}}, \tag{B6}$$

$$H^{(4)}_{\lambda\lambda'\lambda''\lambda'''} = \frac{\hbar^2}{2^2 \times 24 N_c} \Delta_{\mathbf{k}+\mathbf{k}'+\mathbf{k}''+\mathbf{k}''',\mathbf{G}} \frac{V^{(4)}_{\lambda\lambda'\lambda''\lambda'''}}{\sqrt{\omega_\lambda \omega_{\lambda'} \omega_{\lambda''} \omega_{\lambda'''}}}, \tag{B7}$$

$$H^{(iso)}_{\lambda\lambda'} = -\frac{1}{4N} \sum_{l,b} \sum_{\mathbf{k}_l} \Delta m_{l,b} \sqrt{\omega_\lambda \omega_{\lambda'}} \Delta_{\mathbf{k}+\mathbf{k}'+\mathbf{k}_l,\mathbf{G}} \mathbf{e}^\lambda_b \cdot \mathbf{e}^{\lambda'}_b e^{-i\mathbf{k}_l \cdot \mathbf{r}_l}, \tag{B8}$$

$$V^{(3)}_{\lambda\lambda'\lambda''} = \sum_{b,l'b',l''b''} \sum_{\alpha\alpha'\alpha''} \Phi^{\alpha\alpha'\alpha''}_{0b,l'b',l''b''} \frac{e^\lambda_{\alpha b} e^{\lambda'}_{\alpha' b'} e^{\lambda''}_{\alpha'' b''}}{\sqrt{\bar{m}_b \bar{m}_{b'} \bar{m}_{b''}}} e^{i\mathbf{k}'\mathbf{r}_{l'}} e^{i\mathbf{k}''\mathbf{r}_{l''}}, \tag{B9}$$

$$V^{(4)}_{\lambda\lambda'\lambda''\lambda'''} = \sum_{b,l'b',l''b'',l'''b'''} \sum_{\alpha\alpha'\alpha''\alpha'''} \Phi^{\alpha\alpha'\alpha''\alpha'''}_{0b,l'b',l''b'',l'''b'''} \cdot \frac{e^\lambda_{\alpha b} e^{\lambda'}_{\alpha' b'} e^{\lambda''}_{\alpha'' b''} e^{\lambda'''}_{\alpha''' b'''}}{\sqrt{\bar{m}_b \bar{m}_{b'} \bar{m}_{b''} \bar{m}_{b'''}}} e^{i\mathbf{k}'\cdot\mathbf{r}_{l'}} e^{i\mathbf{k}''\cdot\mathbf{r}_{l''}} e^{i\mathbf{k}'''\cdot\mathbf{r}_{l'''}}. \tag{B10}$$

* Electronic address: ruan@purdue.edu

1 A. K. Geim and K. S. Novoselov, Nature materials **6**, 183 (2007), ISSN 1476-1122, URL http://www.ncbi.nlm.nih.gov/pubmed/17330084.

2 Y. Wang, A. K. Vallabhaneni, B. Qiu, and X. Ruan, Nanoscale and Microscale Thermophysical Engineering **18**, 155 (2014), ISSN 1556-7265, URL http://www.tandfonline.com/doi/abs/10.1080/15567265.2014.891680.

3 D. L. Nika and A. A. Balandin, Journal of physics. Condensed matter : an Institute of Physics journal **24**, 233203 (2012), ISSN 1361-648X, URL http://www.ncbi.nlm.nih.gov/pubmed/22562955.

4 Y. Xu, Z. Li, and W. Duan, Small **10**, 2182 (2014), ISSN 1613-6829, URL http://dx.doi.org/10.1002/smll.201303701.

5 K. S. Novoselov, A. K. Geim, S. V. Morozov, D. Jiang, Y. Zhang, S. V. Dubonos, I. V. Grigorieva, and A. A. Firsov, Science (New York, N.Y.) **306**, 666 (2004), ISSN 1095-9203, URL http://www.ncbi.nlm.nih.gov/pubmed/15499015.

6 Y. Zhang, Y.-W. Tan, H. L. Stormer, and P. Kim, Nature **438**, 201 (2005).

7 A. A. Balandin, S. Ghosh, W. Bao, I. Calizo, D. Teweldebrhan, F. Miao, and C. N. Lau, Nano letters **8**, 902 (2008), ISSN 1530-6984, URL http://www.ncbi.nlm.nih.gov/pubmed/18284217.

8 X. Xu, L. F. C. Pereira, Y. Wang, J. Wu, K. Zhang, X. Zhao, S. Bae, C. Tinh Bui, R. Xie, J. T. L. Thong, et al., Nature Communications **5**, 3689 (2014), ISSN 2041-1723, URL http://www.nature.com/doifinder/10.1038/ncomms4689.

9 S. Chen, Q. Wu, C. Mishra, J. Kang, H. Zhang, K. Cho, W. Cai, A. a. Balandin, and R. S. Ruoff, Nature materials **11**, 203 (2012), ISSN 1476-1122, URL http://www.ncbi.nlm.nih.gov/pubmed/22231598.

10 R. R. Nair, P. Blake, A. N. Grigorenko, K. S. Novoselov, T. J. Booth, T. Stauber, N. M. R. Peres, and A. K. Geim, Science **320**, 1308 (2008), http://www.sciencemag.org/content/320/5881/1308.full.pdf, URL http://www.sciencemag.org/content/320/5881/1308.abstract.

11 C. Lee, X. Wei, J. W. Kysar, and J. Hone, Science **321**, 385 (2008), http://www.sciencemag.org/content/321/5887/385.full.pdf, URL http://www.sciencemag.org/content/321/5887/385.abstract.

12 C. Faugeras, B. Faugeras, M. Orlita, M. Potemski, R. R. Nair, and A. K. Geim, ACS Nano **4**, 1889 (2010), pMID: 20218666, http://dx.doi.org/10.1021/nn9016229, URL http://dx.doi.org/10.1021/nn9016229.

13 S. Ghosh, I. Calizo, D. Teweldebrhan, E. P. Pokatilov, D. L. Nika, A. A. Balandin, W. Bao, F. Miao, and C. N. Lau, Applied Physics Letters **92**, 151911 (2008), URL http://scitation.aip.org/content/aip/journal/apl/92/15/10.1063/1.2907977.

14 S. Ghosh, W. Bao, D. L. Nika, S. Subrina, E. P. Pokatilov, C. N. Lau, and A. A. Balandin, Nature materials **9**, 555 (2010), ISSN 1476-1122, URL http://www.ncbi.nlm.nih.gov/pubmed/20453845.

15 P. Goli, H. Ning, X. Li, C. Y. Lu, K. S. Novoselov, and A. A. Balandin, Nano letters **14**, 1497 (2014), ISSN 1530-6992, URL http://www.ncbi.nlm.nih.gov/pubmed/24555640.

16 T. Feng and X. Ruan, Journal of Nanomaterials **2014**, 206370 (2014), ISSN 1687-4110, URL http://www.hindawi.com/journals/jnm/2014/206370/.

17 L. Lindsay and D. A. Broido, Physical Review B **81**, 205441 (2010), ISSN 1098-0121, URL http://link.aps.org/doi/10.1103/PhysRevB.81.205441.

18 B. Qiu and X. Ruan, arXiv preprint arXiv:1111.4613 (2011), arXiv:1111.4613v1, URL http://arxiv.org/abs/1111.4613v1.

19 H. Zhang, G. Lee, and K. Cho, Phys. Rev. B **84**, 115460 (2011), URL http://link.aps.org/doi/10.1103/PhysRevB.84.115460.

20 B. Qiu, Y. Wang, Q. Zhao, and X. Ruan, Applied Physics Letters **100**, 233105 (2012), URL http://scitation.aip.org/content/aip/journal/apl/100/23/10.1063/1.4725194.

21 V. K. Tewary and B. Yang, Phys. Rev. B **79**, 125416 (2009), URL http://link.aps.org/doi/10.1103/PhysRevB.79.125416.

22 L. Lindsay, D. A. Broido, and N. Mingo, Physical Review B **82**, 115427 (2010), ISSN 1098-0121, URL http://link.aps.org/doi/10.1103/PhysRevB.82.115427.

[23] L. Lindsay, D. Broido, and N. Mingo, Physical Review B **80**, 125407 (2009), ISSN 1098-0121, URL http://link.aps.org/doi/10.1103/PhysRevB.80.125407.

[24] D. L. Nika, S. Ghosh, E. P. Pokatilov, and A. A. Balandin, Applied Physics Letters **94**, 203103 (2009), URL http://scitation.aip.org/content/aip/journal/apl/94/20/10.1063/1.3136860.

[25] T. Feng, X. Ruan, Z. Ye, and B. Cao, Phys. Rev. B **91**, 224301 (2015), URL http://link.aps.org/doi/10.1103/PhysRevB.91.224301.

[26] T. Feng and X. Ruan, Physical Review B **93**, 045202 (2016), ISSN 2469-9950, URL http://link.aps.org/doi/10.1103/PhysRevB.93.045202.

[27] T. Feng, L. Lindsay, and X. Ruan, Physical Review B **96**, 161201 (2017), ISSN 2469-9950, URL https://journals.aps.org/prb/abstract/10.1103/PhysRevB.96.161201.

[28] M. Omini and A. Sparavigna, Physica B: Condensed Matter **212**, 101 (1995), ISSN 09214526, URL http://linkinghub.elsevier.com/retrieve/pii/0921452695000163.

[29] J. M. Ziman, *Electrons and Phonons* (Oxford University Press, London, 1960).

[30] M. Kaviany, *Heat Transfer Physics* (Cambridge University Press, New York, 2008).

[31] P. Klemens, *Solid State Physics*, vol. 7 (Academic Press Inc., New York, USA, 1958).

[32] C. de Tomas, A. Cantarero, A. F. Lopeandia, and F. X. Alvarez, Journal of Applied Physics **115**, 164314 (2014), ISSN 0021-8979, URL http://scitation.aip.org/content/aip/journal/jap/115/16/10.1063/1.4871672.

[33] D. Broido, A. Ward, and N. Mingo, Physical Review B **72**, 014308 (2005), ISSN 1098-0121, URL http://link.aps.org/doi/10.1103/PhysRevB.72.014308.

[34] A. Cepellotti and N. Marzari, Physical Review X **6**, 041013 (2016), ISSN 2160-3308, 1603.02608, URL http://arxiv.org/abs/1603.02608.

[35] M. Gill-Comeau and L. J. Lewis, Applied Physics Letters **106**, 193104 (2015), ISSN 0003-6951, URL http://scitation.aip.org/content/aip/journal/apl/106/19/10.1063/1.4921127.

[36] M. Gill-Comeau and L. J. Lewis, Physical Review B **92**, 195404 (2015), ISSN 1098-0121, URL http://link.aps.org/doi/10.1103/PhysRevB.92.195404.

[37] N. Bonini, J. Garg, and N. Marzari, Nano letters **12**, 2673 (2012), ISSN 1530-6992, URL http://www.ncbi.nlm.nih.gov/pubmed/22591411.

[38] S. Lee, D. Broido, K. Esfarjani, and G. Chen, Nature Communications **6**, 6290 (2015), ISSN 2041-1723, URL http://www.nature.com/doifinder/10.1038/ncomms7290.

[39] A. Cepellotti, G. Fugallo, L. Paulatto, M. Lazzeri, F. Mauri, and N. Marzari, Nature Communications **6**, 6400 (2015), ISSN 2041-1723, URL http://www.nature.com/doifinder/10.1038/ncomms7400.

[40] L. Lindsay, W. Li, J. Carrete, N. Mingo, D. A. Broido, and T. L. Reinecke, Physical Review B **89**, 155426 (2014), ISSN 1098-0121, URL http://link.aps.org/doi/10.1103/PhysRevB.89.155426.

[41] G. Fugallo, A. Cepellotti, L. Paulatto, M. Lazzeri, N. Marzari, and F. Mauri, Nano letters **14**, 6109 (2014), ISSN 1530-6992, URL http://www.ncbi.nlm.nih.gov/pubmed/25343716.

[42] H. Xie, L. Chen, W. Yu, and B. Wang, Applied Physics Letters **102**, 111911 (2013), ISSN 00036951, URL http://link.aip.org/link/APPLAB/v102/i11/p111911/s1{&}Agg=doi.

[43] Q.-Y. Li, K. Takahashi, H. Ago, X. Zhang, T. Ikuta, T. Nishiyama, and K. Kawahara, Journal of Applied Physics **117**, 065102 (2015), ISSN 0021-8979, URL http://scitation.aip.org/content/aip/journal/jap/117/6/10.1063/1.4907699.

[44] S. Chen, A. L. Moore, W. Cai, J. W. Suk, J. An, C. Mishra, C. Amos, C. W. Magnuson, J. Kang, L. Shi, et al., ACS Nano **5**, 321 (2011), pMID: 21162551, http://dx.doi.org/10.1021/nn102915x, URL http://dx.doi.org/10.1021/nn102915x.

[45] J.-U. Lee, D. Yoon, H. Kim, S. W. Lee, and H. Cheong, Phys. Rev. B **83**, 081419 (2011), URL http://link.aps.org/doi/10.1103/PhysRevB.83.081419.

[46] A. K. Vallabhaneni, D. Singh, H. Bao, J. Murthy, and X. Ruan, Physical Review B **93**, 125432 (2016), ISSN 2469-9950, URL http://link.aps.org/doi/10.1103/PhysRevB.93.125432.

[47] Z. Fan, L. F. C. Pereira, H.-Q. Wang, J.-C. Zheng, D. Donadio, and A. Harju, Physical Review B **92**, 094301 (2015), ISSN 1098-0121, URL http://link.aps.org/doi/10.1103/PhysRevB.92.094301.

[48] Z. Fan, L. F. C. Pereira, P. Hirvonen, M. M. Ervasti, K. R. Elder, D. Donadio, T. Ala-Nissila, and A. Harju, Physical Review B - Condensed Matter and Materials Physics **95**, 1 (2017), ISSN 1550235X, 1612.07199.

[49] J. Turney, A. McGaughey, and C. Amon, Physical Review B **79**, 224305 (2009), ISSN 1098-0121, URL http://link.aps.org/doi/10.1103/PhysRevB.79.224305.

[50] L. Lindsay, D. a. Broido, and N. Mingo, Physical Review B **83**, 235428 (2011), ISSN 1098-0121, URL http://link.aps.org/doi/10.1103/PhysRevB.83.235428.

[51] A. Maradudin and A. Fein, Physical Review **128**, 2589 (1962), URL http://prola.aps.org/abstract/PR/v128/i6/p2589_1.

[52] S.-i. Tamura, Physical Review B **27**, 858 (1983), URL http://journals.aps.org/prb/abstract/10.1103/PhysRevB.27.858.

[53] H. B. G. Casimir, Physica **5**, 495 (1938), provided by the SAO/NASA Astrophysics Data System, URL http://adsabs.harvard.edu/abs/1938Phy.....5..495C.

[54] R. Berman, F. E. Simon, and J. M. Ziman, Proceedings of the Royal Society of London A: Mathematical, Physical and Engineering Sciences **220**, 171 (1953), ISSN 0080-4630, URL http://rspa.royalsocietypublishing.org/content/220/1141/171.

[55] R. Berman, E. L. Foster, and J. M. Ziman, Proceedings of the Royal Society of London. Series A, Mathematical and Physical Sciences **231**, 130 (1955), URL http://www.jstor.org/stable/99632.

[56] M. Omini and A. Sparavigna, Nuovo Cimento della Societa Italiana di Fisica D **19D**, 1537 (1997), ISSN 03926737, URL http://www.sif.it/riviste/ncd/econtents/1997/019/10/article/5.